Original Research Article

Network-based modeling of biogas consumption prediction in a cook stove model

Abstract

This study seeks to propose a new model of hearth for the consumption of biogas produced by a biodigester of 4 m3. The cylindrical furnace is used to heat an empty pot for 3 hours. To do this, the system is subdivided into two sub-systems, the first of which is the flame, which then heats the bottom of the pot. The latter is the second hottest point. The developed network is composed of 8 isothermal points, interconnected by thermal resistances, each of which represents a particular type of heat transfer mode. The resolution of the system required 8 differential equations. The modeling allowed us to appreciate the temperatures governing the system. The experimental study proves an agreement with the model temperatures. Studies show that the optimal thickness and height of the hearth are respectively 12mm and 10 cm. The heat ide the internal air of the kettle is 220°C and the flame temperature is 900℃. The instantaneous efficiency of the firebox obtained is 65. In addition, a validation with literature data to confirm this study, therefore its adoption will lead to reducing the consumption of biogas and therefore have a positive impact on the woodcut.

Keywords: Biogas, fireplace, energy performance

1 Introduction

Animal manure represents a large source of value in methanization given the high number of farms and the importance of livestock in the country. It is the first resource used in agricultural methanisation, especially in small biodigesters (Whitman et al., 2011). In Burkina Faso the livestock (cattle, sheep, goat, camel, pig) amounts to 32850000 in 2022,(Ceballos et al. 2015) the biogas technology is a very attractive way to use on this biomass to meet partial energy needs. In fact, the proper functioning of the biogas system can offer multiple benefits to users and as a result the conservation and protection of environmental resources. In the work of Achinas (Achinas, Achinas, and Euverink 2017), they have shown that the use of this type of waste in methanization reduces the powerful greenhouse gas (CH4) that can escape into the atmosphere without being converted into carbon dioxide(Saber et al. 2021. This technology must be accompanied by a less energy-consuming furnace. The hearth is cylindrical in shape with a burner containing a 3.5 mm nozzle. The study focuses on modeling by the thermal network approach and experimentation. To do so, differential systems of equations governing heat transfer in the considered furnace configurations have been set up and used to evaluate the node temperature systems and their efficiency. After the methodology of the furnace in section 2, the furnace is modeled and validated in section 3 while section 4 is devoted to the simulation results and discussion.

Abbreviations		
PCI	Power Calorific Value	MJ/L
D	biogas flow	L/S
Cd	coefficent de pertes de charge	J-1
Cp	Chaleur spefique	W(mK)
m	Mass	kg
λ	Thermal conductivity	(W.m-2.K)
p	Density	kg.m3
T	Température	℃,K
β	coefficient of expansion	℃-1
Gr	Nombre de grasoft	Without unit
Nu	Number of nussselt	Without unit
F	Form Factor	Sans unite
Ra	Number of Raleigh	Without unit
Pr	Number of Prandtl	Without unit
p	Pression	atm
Q	Quantity of energy	J
η	energy efficiency	%

2 Materials and Methods

2.1 Presentation of the model

The system is subdivided into two subsystems $\{a, b, c, d, k, h\}$ et $\{d, e, f, g, h\}$ The way it works is that the heat source point exchanges with points a, b, c, d, h, and k. The greatest exchange is with point d which will later become the second hottest point. This last point will exchange vice versa with the points e, f, g, and the ambient medium k. Point d acts as a bridge between the two subsystems. Conduction was studied between h and a, considering the strong heat coming from the burner at point a and the doubled thickness of 14 mm between a and h. The search for the temperature of the internal air of the kettle is the objective of the heating. The physical model and the circuit allowing the discretization of the equations are represented in 1a and 1b.

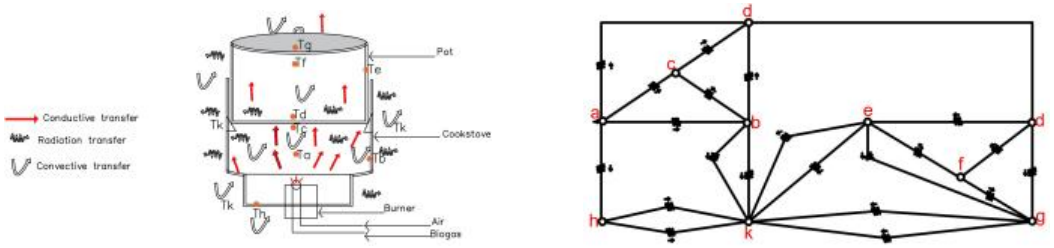

(a) Physical model (b) temperature network

Figure 1: Study method and diagram of the equivalent circuit of the discretization of the hot spots

Simplifying assumptions

To simplify the approach to the heat transfer equations within the furnace, the following assumptions have been made about the steady state

- Air flow is uniform through the burner
- The heat flow and temperature of each component are uniform at each time step
- The volume of air within the pot is constant
- The temperature of the outside air and the fireplace is uniform and identical to that of the groun
- The heat loss around the focus does not affect the ambient temperature
- Mass transfer was not considered in this study
- Only time space was used for discretization.

2.2 Introduction of the cooke stove

The stove is built with a locally available 14 mm thick iron sheet and the pot is made of recycled aluminum. The height of the firebox is 30 cm from the ground. With a 15 cm radius and the height of the combustion chamber is 10 cm playing the role of the tunnel that can lead the hot gases to the pot. It is designed in two levels, the first one is the combustion chamber with a diameter of 10 cm and the second one allows it to fit the pot with a thickness of 2 cm. A pot with a radius of 13 cm is made to fit correctly into the firebox to avoid leaks. The pot is fitted with a lid of the same material as the pot with a radius of 14 cm. The lid covers it during the test to fit without any air intake gap. The system is running because of the biogas fed from the biodigester with a pipe allowing combustion in a 3.5 mm diameter nozzle burner. The hearth device is present in figure 2a and that of the whole device de2b for testing.

Fuel Quantity Calculation

The fuel enters the furnace through the 3.5 mm nozzle. This amount is calculated according to Bernoulli's theorem equation in fluids(Kurchania et al., 2010). With D, nozzle diameter (mm), p the pressure (kPa) and the density of the biogas ($kg.m^{-3}$). The discharge coefficient of 0.9 is obtained from the Bernoulli diagram. The oxygen volume is calculated with the stoichiometric equation representing the biogas volume. The equation 2.2 describes biogas consumption.

$$debit_{biogaz} = 0,036.Cd.D^2.\sqrt{\frac{p}{\rho}} \tag{2.1}$$

The loss coefficient is introduced to account for all the inefficiencies of the flow tube effect whose value is $\in [0; 1]$ according to the work of petoro (Petro et al., 2020)

$$q_{comb} = debit_{biogaz} PCI \tag{2.2}$$

Numerical study of the thermal efficiency of the fireplace

The instantaneous efficiency is determined by considering the quotient of all the energies arriving on the kettle as useful energy by the energy of combustion. The energy received by the pot is given by:

(a) [Study cook stove (b) Experimentation with the fireplace

Figure 2: Type of Home and the complete experimentation device

$$Qu = \frac{[m_{pot}cp_{pot}(T_d - T_0) + m_{pot}cp_{pot}(T_e - T_0) + m_{air2}cpair2(T_f - T_0) + m_{\text{cover}}cp_{\text{cover}}(T_g - T_0)]}{temps} \tag{2.3}$$

$T_0)$ is the value of the initial temperature which is at the same time the ambient value. The yield is now given by:

$$\eta = \frac{Qu}{q_{comb}}.100 \tag{2.4}$$

This function is entered into the program with the same time step as the temperature calculations.

Thermal exchange at the flame

The conservation equation of energy from burning biogas to heat the combustion chamber is:

$$m_{comb}\text{Cp}_{comb} * \frac{dT_a}{dt} = \left[\begin{array}{l} A_1F_{12} * \sigma({T_b}^d - T_a^4) + + h_1A_1(T_c - T_a) + \\ + A_1F_{12} * \sigma({T_d}^4 - T_a^4) + + U_{1-8}A_1(T_d - T_1^4) + q_{comb} \end{array} \right] \tag{2.5}$$

The combustion of gas is an exothermic process as a whole. The heat produced is in the 900 ℃ range. Thus, the energy quantity of combustion is calculated according to the equation 2.2.The specific heat of air mixing with biogas 0.9536 kJ/kg/℃ is obtained according to the work of Augustin (Augustin et al., 2022).

Heat exchange at the hearth wall

The temperature of the wall of the furnace is close to the flame and calculated according in 2.6..

$$m_{w1}\mathrm{Cp}_{w1}\frac{dT_b}{dt} = \left[\begin{array}{l} A_2F_{21}\sigma({T_a}^4 - T_b^4) + h_1A_2(T_c - T_b) + \\ +A_2F_{24}\sigma({T_d}^4 - T_b^4) + h_3A_3(T_k - T_b) \\ +A_3({T_k}^4 - T_b^4) \end{array}\right] \tag{2.6}$$

Heat exchange at the combustion chamber

the heat balance in the combustion chamber is described in the equation 2.7.

$$m_{air,1}\mathrm{Cp}_{air,1}\frac{dT_c}{dt} = [h_1A_1(T_a - T_c) + h_1A_2(T_a - T_c) + h_1A_4(T_a - T_c)] \tag{2.7}$$

Heat exchange at the base of the kettle

The base of the firebox is the part in direct contact with the flame and the equation is presented in 2.8

$$m_{pot}\mathrm{Cp}_{pot}\frac{dT_d}{dt} = \left[\begin{array}{l} A_2F_{41}\sigma.({T_a}^4 - T_d^4) + h_1.A_4(T_c - T_d) + \\ +A_2F_{42}\sigma.({T_b}^4 - T_d^4) + A_5F_{45}\sigma.({T_e}^4 - T_d^4) + \\ +h_2A_5.(T_f - T_b) + A_5F_{47}\sigma.({T_g}^4 - T_d^4) \end{array}\right] \tag{2.8}$$

Thermal exchanges at the level of the thickness of the pot

The energy balance between the walls of the pot and the other points is presented by 2.9.

$$m_{pot}\mathrm{Cp}_{pot}\frac{dT_e}{dt} = \left[\begin{array}{l} A_6F_{54}\sigma({T_d}^4 - T_e^4) + h_2 * A_6(T_f - T_e) + \\ +A_6F_{57}\sigma * ({T_g}^4 - T_e^4) + A_7F\sigma({T_k}^4 - T_e^4) + \\ +h_3A_7 * (T_k - T_e) \end{array}\right] \tag{2.9}$$

Heat exchange inside the pot

The pot is empty, the air is heated whose energy balance equation is 2.10.

$$m_{air,2}\mathrm{Cp}_{air,2}\frac{dT_f}{dt} = [h_2A_5(T_d - T_f) + h_2A_2(T_e - T_f) + h_2A_8(T_g - T_f)] \tag{2.10}$$

Heat exchange at the pot lid

The heat balance on the lid of the pot is given in 2.11.

$$m_{\mathrm{cover}}\mathrm{Cp}_{\mathrm{cover}}\frac{dT_g}{dt} = \left[\begin{array}{l} h_2A_8(T_f - T_g) + A_8F_{75}\sigma({T_e}^4 - T_g^4) + A_9F\sigma({T_k}^4 - T_g^4) + \\ +A_8F_{74}\sigma * ({T_d}^4 - T_g^4) + h_3A_9(T_k - T_g) \end{array}\right] \tag{2.11}$$

Heat exchange at the base of the fireplace

The lining of the base of the fireplace reduces the heat transfer from the burner to the bottom of the fireplace. The energy balance at the bottom of the fireplace, i.e. the most insulated part of the fireplace, is presented in 2.12.

$$\mathrm{m}_{w,2}\mathrm{Cp}_{w,2}\frac{dT_h}{dt} = \left[h_2A_8(T_k - T_h) + A_8F\sigma({T_k}^4 - T_h^4)\right] \tag{2.12}$$

$$Cp\_air_1 = (0.9362 + 0.0002 * (Ta\,(i))) \tag{2.13}$$

Determining the constants

The resolution of the equations requires thermal coefficients. There are three modes of heat transfer and three coefficients of exchange. For the conduction considered at the bottom of the focus, the equation is shown in 2.14.

$$U_{1-8} = \frac{K_{foyer}}{e_{base}} \tag{2.14}$$

With K_{foyer},the conductivity of iron and e_{base} the thickness of the focus.
The form factor to calculate the radiation coefficient between two points i and j is given by 2.15.

$$F_{ij}eq = \frac{1}{\frac{1}{\varepsilon_i} - 1 + \frac{1}{F_{ij}} + \frac{S_i}{S_j}\left(\frac{1}{\varepsilon_i} - 1\right)} \tag{2.15}$$

F_{ij} represents the geometric form factors between the surface of S_i et S_j; ε_i, ε_j are the permissivities of the surfaces . The focus is considered as a black body so ε is 1 and that of the pot (aluminum) is 0.8. After reduction, the radiative exchange coefficient between two bridges becomes

$$hr_{i-j} = \sigma\varepsilon({T_i}^2 + {T_j}^2) * (T_i + T_j) \tag{2.16}$$

and the convective exchange coefficient between the fluid and the faces is given by the formula With K_{air} the conductivity of the air and L the length of the wall. the combustion chamber is in the form of a tube whose diameter is smaller than its length. In natural convection, the Nusselt number is given by the relation:

$$Nu_1 = 0,023.Re^{0,8}(1 + (D/L))^{(0.7)}.0,685^{(1/3)} \tag{2.17}$$

The interior of the kettle and the surrounding environment are in natural convection and in a laminar regime so the Nusseelt number is given by the relation 2.18. This relation is used in the framework of a free jet touching a plane surface that we assumed for the exterior and the interior of the kettle(Zube et al., 2021).

$$Nu_2 = 0,54(Gr.\,\mathrm{Pr})^{(0.25)} \tag{2.18}$$

The number of Grassoft is calculated by the relation:

$$Gr = \frac{g.\beta.T.L^3.\rho^2}{\mu^2} \tag{2.19}$$

the number of prandlt is given:

$$Pr = \frac{\mu.Cp}{k} \tag{2.20}$$

The thermal expansion is obtained by:

$$\beta = 1./T \tag{2.21}$$

Of which μ,dynamic viscosity, υ the kinematic viscosity, $C_p$the specific heat and ρ the density. H is the convection exchange coefficient.

$$h = \frac{Nu.k}{L} \tag{2.22}$$

2.3 Validation of the model

The numerical validation consisted in retrieving the author's numerical data and finding a polynomial equation describing these data(Tampango et al., 2011) according to 2.23.

$$y = a_n x^n + a_{n-1}x^{n-1} + a_1 x^1 + ... + a_0 \tag{2.23}$$

With a the coefficients and n the degree of the polynomial. This polynomial is implemented under Matlab in order to determine the errors committed on the results with the static formula RMSE (Root Mean Square Eroor)(Guermoui et al., 2022) present in 2.24

$$RMSE = \sqrt{\frac{1}{N}\sum_{1}^{N}\left(y_{\exp}(t_i) - y_{sim}(t_i)\right)^2} \tag{2.24}$$

yexp are the collected measurements, , ysim are the data predicted by the model, θ represents the parameters to be determined and N is the number of measurements.

3 Results and Discussion

3.1 presentation of results

The figures 3,4, 5,6, show the evolution of the experimental and simulation temperatures over time. The results are the flame temperature Ta, the wall temperature Tb, the combustion chamber temperature Tc, the bottom temperature td, the thickness of the pot Te. Also the lid temperature Tg, inner pot temperature Tf and the bottom temperature of the furnace Th.

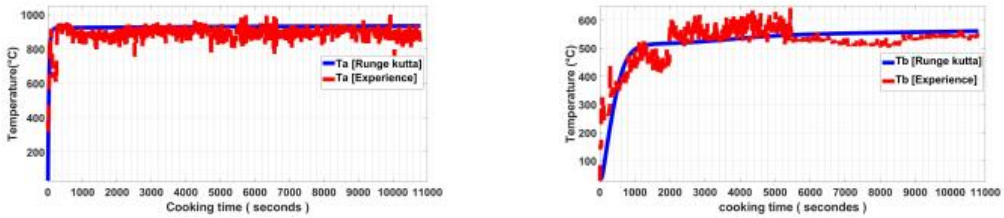

(a) Flame (b) cooker wall

Figure 3: Temperatures of the flame and the thickness of the hearth

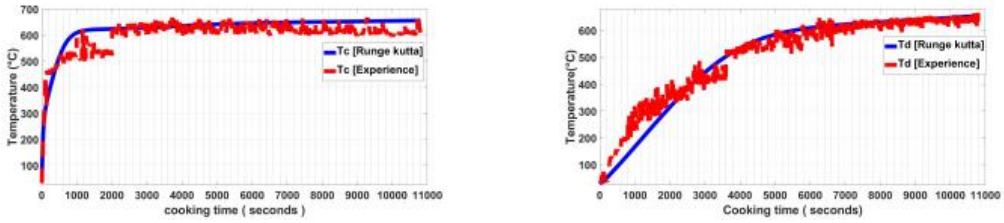

(a) Combustion chamber (b) pot base wall

Figure 4: Temperatures of the combustion chamber and the base of the pot

The Ta at t=0s Ta is 27 °C increases to 900 °C at t= 500 Seconds and remains stable. The temperature Tb of the wall is t = 2000s at 400 °C, then continues to grow to stabilize at Tb = 500 °C

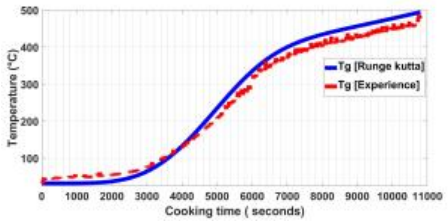

(a) lid

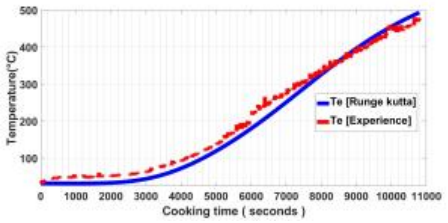

(b) vertical wall of the po

Figure 5: Temperatures of the lid and the base of the pot

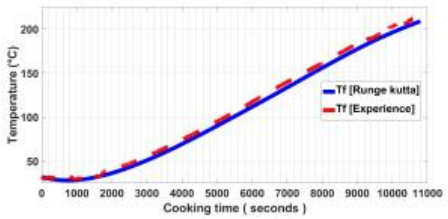

(a) internal pot temperature

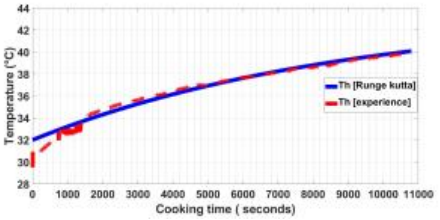

(b) base wall of the fireplace

Figure 6: Internal air temperatures of the pot and the base of the fireplace

from 1000 seconds. The experimental Ta = 895 °C at t = 7000s, simulated Ta =900 °C in the same way experimental Tb = 465 °C compared Tb =500 °C at t =2000s.We notice that the experimental and simulated data are in agreement. This high flame temperature results from the fact that the heating value=$36MJ/m^3$ of methane which is the main component of biogas is very high i.e. a methane composition of 60%. This heat flow touches the wall considering the radius of the chamber is reduced to 13 cm. Thus, it increases the temperature Tb which reaches 500 °C. Also, the thickness e = 14 mm of the hearth has a strong influence on the temperature Tb. The large thickness has a high thermal inertia, allowing the flame to reach the equilibrium point quickly at 900 °C and the firebox wall at 600 °C. This would explain that once the firebox is overheated, the temperature remains almost constant throughout the rest of the kitchen, showing the stability of the firebox. Bagaya's work (Bagaya et al., 2021) on fireplaces found a temperature of 408.2 °C and sufficient to prepare any type of food. In our study, with this temperature of 900 °C the operator will take less time for cooking the meals which is an advantage. The curves 4b show that the temperature of the adiabatic chamber which is low at the beginning Tc = 35 °C at the t = 10s quickly reaches its maximum at 600 at t = 100s . The experimental part is at t = 1000s in a temperature Tc = 555 °C and the simulated part in this same time is at Tc = 600 °C. The curves in Figure 4b show a slow evolution to reach values to reach its maximum of Td =500 °C at t = 5000s before stabilizing at 500 °C for the rest of the study. We find that the heat transfers in the enclosure are influenced by the increase of the heat flux from the burner. Thus, the hot air from the chamber is directed straight to the base of this pot keeping its temperature high in 600 °C.Moreover, we see that the temperature of the base of the pot presented in figure 2.8 is not different from that of the flame and this explains a good heat transfer to the pot. The curves in Figure 6b show values of Tg = 50 °C on the lid until t = 3000s, then starts to increase to reach Tg = 400 °C

at t = 4000s. The figure shows the evolution of the temperature Te of the thickness of the aluminium pot both experimentally and modelled. At first the temperature remains lower than 100℃ until 5000s. Then it increases slowly to reach 500 °C at the end of the test in 10800 seconds. The curves of figure 5b show for values of Te lower than 100 °C the thickness of the edge in $\Delta t = 0 - 4000s$, then grows to reach Te = 450 °C at t = 3000s. This temperature after the 5000 seconds evolves exponentially to reach a temperature of 450 °C in three hours. These temperatures around 500 °C mean that the hot gas flow inside the chamber is not affected by the external environment as shown in figure 5b. The figures 6a from the experiment and modeling of the temperature Tf with time. the Tf in figure 6a grows to reach 220 °C at t = 1000s and the Th shown in 6 give 36 °C at t=2000s, then grows slightly to reach 50 °C. The experimental and simulation data remain similar during the three hours of combustion. We can say that this temperature Tf of the air at 220 °C at the end of the test in the kettle is sufficient to boil water. The difference in temperature between the flame and within the pot 250 °C at the outlet, clearly shows that the thermal energy was gained by the air inside the pot. In the figure, we can see that whatever the temperature of the hot spots, the temperature at the bottom of the fireplace remains low around 65 °C. This result shows that the temperature inside the fireplace does not influence the heat exchange between the base of the fireplace which is placed on the ground and the inside of the fireplace. This good result is allows to reduce the heat loss which is the problem of open fireplaces (Gandigude and Nagarhalli, 2018). It is justified by the position of the burner being 10 cm above the base. Also the base thickness of the fireplace is doubled by 14 mm explaining these similar results of simulation and experimentation. The purpose of a fireplace is to transmit a maximum of heat to the contents of the pot. Unfortunately, the combustion cannot be adiabatic and the burnt gases lose enthalpy at the walls and by radiation. In our study, we obtained a good prediction of heat loss reduction. With this model, the external temperature of the furnace is around 60 °C which an advanced and similar to the work of SagouongSagouong and 2018 whose result of the wall loss Th is 80 °C.

3.2 Study validation

The figure represents the evolution of the flame temperature along the test compared to the study of sagnoung1 modeled with the Runge Kutta method. The Ta at t = 100 seconds for our study is 800K and 799K for the author's study. At t = 600s the temperature of the sagnoug flame is 805K, 802K for our study and the whole stabilizes around 800K. The firebox designed by this author is made of aluminum using the Runge Kutta method with a cylindrical shape. The comparison of the calculation error between the two studies is 0.4 K. We notice that the simulated curve admits the same shape as that obtained by Sagouong(Sagouong ,Tchuen, 2018) proving the effectiveness of the Runge Kutta model. The curves in Figure 9b show the efficiency of our study and that of Khaushik as a function of time t. At t= 0s the η are 0%, 15% respectively for our study and the author's. At t = 6000s the performance of our study is 50% and that of Khaushik (Kaushik, 2019) is 49%. The difference observed with the work of the first author Sagnoug is at the level of the heat source. Our study concerned biogas whereas that of the latter concerns coal whose PCI is largely lower than that of the gas. Consequently, the temperature of the flame of this last is less around 800K compared to that of the biogas with 1100K.
The work of Khausik (Kaushik, 2019) is based on a numerical model on CFD software whose focus is covered with ceramic with a thickness of 10 mm. This parameter would justify this better result of 70% compared to ours in either CFD method. Indeed, the error (RMSE) between our results is 4.1An experiment was used to see the reliability of our study. A variation from 900 ℃ to 850 °C is observed in a few seconds. This difference is due to the phenomenon of the wind creating sometimes a vortex effect in the combustion chamber. Overall, the values predicted by the model are acceptable and can help to design an efficient fireplace.

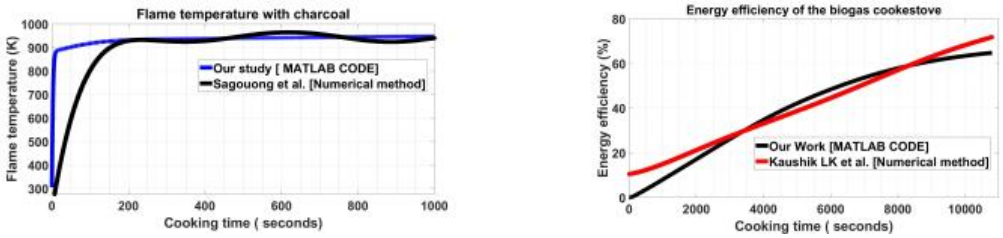

(a) Flame (b) combustion chamber

Figure 7: Validation of the flame temperatures with the numerical model of sagnoug et al and of the thermal efficiency of the firebox with the Khaushik model LK et al

3.3 Influence of focus thickness

A variation in the thickness of the fireplace leads to a significant variation in the energy performance of the fireplace. The figure 8b shows the influence of thickness on the energy loss at the base and Figure 8a the thermal efficiency. For thicknesses greater than 14m the yield is around 80 % and the base temperature is 40 °C. On the other hand, a thickness of less than 10 mm results in an efficiency

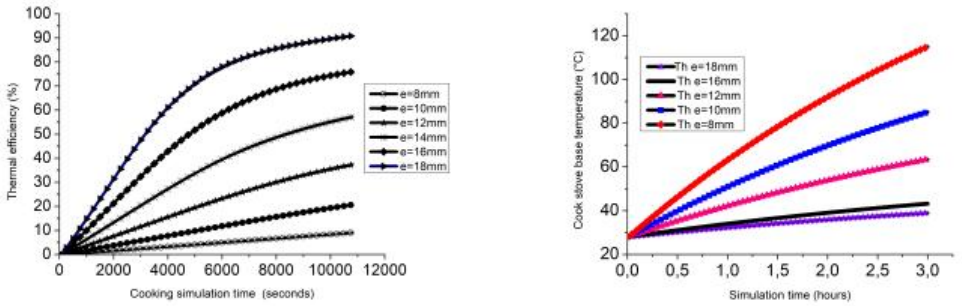

(a) Thermal efficiency (b) Insulation temperature

Figure 8: Internal air temperatures of the pot and the base of the fireplace

of 25 % and a loss of up to 100 °C. The reason behind this is that there is more heat loss (convective and radiative heat) with a small hearth resulting in lower thermal efficiency and more heat loss to the environment with a large vessel. The Th temperature we studied conduction in order to see the influence of the thickness on the thermal behavior of the hearth. For the thickness of 8 mm the Th temperature is at 115 °C at t = 3h and for a thickness of 10 mm the temperature of the base is at 80 °C at the end of the test of 10800 seconds. This can also be explained by the fact that the heat transfer by conduction between the center of the hearth enclosure and the hearth wall becomes weak if the thickness of the hearth is high and strong if the thickness becomes increasingly strong.

3.4 Influence of combustion chamber height

The figures 9 show the evolution of the temperature in the kettle and the efficiency as a function of time. We notice that when we increase the height of the combustion chamber, the flame does

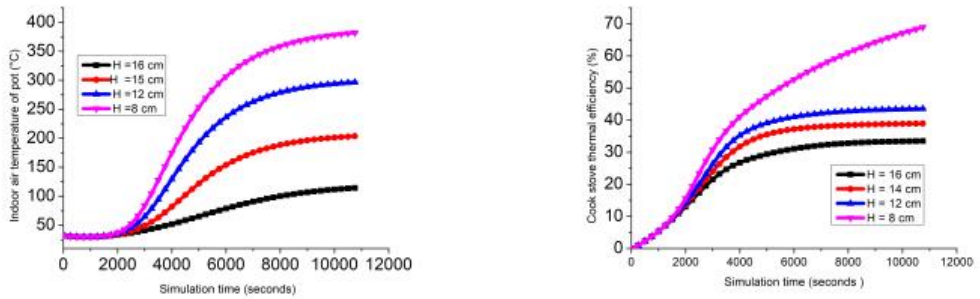

(a) within the pot (b) Thermal efficiency

Figure 9: Impact of chamber height on internal pot temperature and energy efficiency

not reach the base of the pot. This results in a large surface area of the chamber being covered reducing the wall temperatures. Therefore, an increase in the height of the combustion chamber leads to a reduction in thermal efficiency. With a height of 12 cm, the temperature at the bottom of the pot increases from 900 to 800 °C and the heat inside the pot decreases from 225 to 140 °C . The combustion chamber at a height of 10 cm is ideal for maintaining this performance and prevents the pot from smothering the flame. These results show that as the height of the combustion chamber increases, the thermal efficiency decreases. As the height increases, the combustion produced does not interact with the bottom of the pot. At the same time, the air inside also tends to cool down due to the contact with the ambient air. On the other hand, the decrease in the flame height increases the impact of the flame on the vessel, which increases the contact surface between the flame and the vessel. As a result, the thermal efficiency of the burner increases, indicating a phenomenon of heat transfer by convection in the pot chamber. For heights of 12 cm, η = 40% and 8 cm η = 80%. This is because the thermal gradient transferred to the pot at this height remains high.

4 CONCLUSIONS

This work was to propose a model with a higher energy efficiency that can be easily adopted by users of biodigesters. To achieve a good result we have thus presented a method of modeling and simulation of the prototype and then validate the behavior of the complete system in the MATLAB/Simulink environment. The studied furnace is of cylindrical shape for vacuum combustion. The results obtained from the developed model are in agreement with the experimental data. It was found that the model provides a prediction of temperature within the pot that can reach 220 °C that can cook a meal. Then the evolution of the temperature is under the influence of the thickness of the focus during the time from t = 0s to the final time tf = 10800s . From the numerical results on the focus, in figure 3a, we see that the highest temperature is Ta = 900 °C followed by Tb = 600 °C in figure 3b. This is favored by the source which is hot and sweeps the wall thus testifying to these high temperatures. We notice

that the lowest temperatures are those of the air inside the pot 225 °C and the temperature of the base of the pot 65 °C. The instantaneous efficiency of the furnace is 65%. All the results presented describe the system behavior almost perfectly and therefore acceptable according to the literature (Grimm, 2014).

References

Achinas, Spyridon, Vasileios Achinas, and Gerrit Jan Willem Euverink. 2017. “A Technological Overview of Biogas Production from Biowaste.” Engineering 3(3): 299–307. http://dx.doi.org/10.1016/J.ENG.2017.03.002.

Augustin, L. M., Vertomene, S. T., Bernard, N. N., Sadiki, A., and Haddy, M. K. (2022). A New Perspective on Cooking Stove Loss Coefficient Assessment by Means of the Second Law Analysis. 1–27.

Bagaya, N., Ouedraogo, I., Windé, D., Koumbem, N., Sandwidi, G. W., and Kieno, F. P. (2021). Energy Performance Analysis of B1-3 . 5mm Burner Model of Fasobio-15 Biodigester Biogas Cookstoves. 25(7), 11–21. https://doi.org/10.9734/PSIJ/2021/v25i730268

Ceballos, Gerardo et al. 2015. “Accelerated Modern Human-Induced Species Losses: Entering the Sixth Mass Accelerated Modern Human – Induced Species Losses: Entering the Sixth Mass Extinction.” (June).

Guermoui, M., Abdelaziz, R., Gairaa, K., Djemoui, L., and Benkaciali, S. (2022). New temperature-based predicting model for global solar radiation using support vector regression. International Journal of Ambient Energy, 43(1), 1397–1407. https://doi.org/10.1080/01430750.2019.1708792

Grimm, M. (2014). Impact Evaluation of Improved Stove Use among Dolo-beer Breweries in Burkina Faso – FAFASO. July 2013, 1–31.

Kaushik, L. K. (2019). Performance and Feasibility Assessment of Porous Radiant Burner Aided Cook-stoves for LPG , Biogas and Waste Cooking Oil Fuels Doctor of Philosophy by Department of Mechanical Engineering Indian Institute of Technology Guwahati Department of Mechanical En. Saber, Meryem et al. 2021. “Enhancement of Organic Household Waste Anaerobic Digestion Performances in a Thermophilic Pilot Digester.” Biomass and Bioenergy 144(July 2020): 105933. https://doi.org/10.1016/j.biombioe.2020.105933.

Kurchania, A-K, Panwar, N. L., and Pagar, S. D. (2010). International Journal of Sustainable Energy Design and performance evaluation of biogas stove for community cooking application Design and performance evaluation of biogas stove for community cooking application. International Journal of Sustainable Energy, 29(2), 116–123. http://www.tandfonline.com/action/journalInformation?journalCode=gsol20

Gandigude, A. and Nagarhalli, M. (2018). ScienceDirect Simulation of Rocket Cook-Stove Geometrical Aspect for its Performance Improvement. Materials Today: Proceedings, 5(2), 3903–3908. https://doi.org/10.1016/j.matpr.2017.11.645

Petro, L. M., Machunda, R., Tumbo, S., and Kivevele, T. (2020). Theoretical and Experimental Performance Analysis of a Novel Domestic Biogas Burner. 2020.

Tampango, Y., Potier-ferry, M., Koutsawa, Y., Tampango, Y., Potier-ferry, M., and Koutsawa, Y. (2011). Une méthode sans maillage basée sur la résolution de l ' EDP par séries de Taylor To cite this version: HAL Id: hal-00592826.

Sagouong, J. M., and Tchuen, G. (2018). Mathematical modelling of traditional stoves using the Thermal Network Approach. April. https://doi.org/10.14445/22315381/IJETT-V58P201

Whitman, T., Nicholson, C. F., Torres, D., and Lehmann, J. (2011). Climate change impact of biochar cook stoves in western kenyan farm households: System dynamics model analysis. Environmental Science and Technology, 45(8), 3687–3694. https://doi.org/10.1021/es103301k

Zube, N. G., Zhang, X., Li, T., Le, T., Li, C., Guerlet, S., and Tan, X. (2021). Radiative-dynamical Simulation of Jupiter's Stratosphere and Upper Troposphere. The Astrophysical Journal, 921(2), 174. https://doi.org/10.3847/1538-4357/ac1e95